Dalton Transactions

ROYAL SOCIETY OF CHEMISTRY

PAPER

View Article Online
View Journal | View Issue

Check for updates

Cite this: *Dalton Trans.*, 2024, **53**, 6791

Photocatalytic conversion of CO_2 to CO by Ru(II) and Os(II) octahedral complexes: a DFT/TDDFT study†

Athanassios C. Tsipis * and Antonia A. Sarantou

Received 15th January 2024,
Accepted 21st March 2024

DOI: 10.1039/d4dt00125g

rsc.li/dalton

The reaction mechanisms of the photocatalytic reduction of CO_2 to CO catalyzed by $[(en)M(CO)_3Cl]$ complexes (M = Ru, Os, en = ethylenediamine) in the presence of triethanolamine (TEOA), R_3N (R = $-CH_2CH_2OH$), in DCM and DMF solvents, were studied by means of DFT/TDDFT electronic structure calculations. The geometric and free energy reaction profiles for two possible reaction pathways were calculated. Both reaction pathways studied, start with the 17e$^-$, catalytically active intermediate, $[(en)M(CO)_3]^{\bullet+}$ generated from the first triplet excited state, T_1 upon reductive quenching by TEOA which acts as a sacrificial electron donor. In the first possible pathway, $TEOA^-$ anion binds to the metal center of the catalytically active intermediate, $[(en)M(CO)_3]^{\bullet+}$ followed by CO_2 insertion into the M-$OCH_2CH_2NR_2$ bond. The latter upon successive protonations releases a metal 'free' $[R_2NCH_2CH_2OC(O)(OH)]$ intermediate which starts a new and final catalytic cycle, leading to the formation of CO and H_2O while regenarating TEOA. In the second possible pathway, the 17e$^-$, catalytically active intermediate, $[(en)M(CO)_3]^{\bullet+}$ captures CO_2 molecule, forming an η^1-CO_2 complex. Upon $2H^+/2e^-$ successive protonations and reductions, CO product is obtained along with regenarating the catalytically active intermediate $[(en)M(CO)_3]^{\bullet+}$. The nature of the proton donor affects the reaction profiles of both mechanisms. The nature of the solvent does not affect significantly the reaction mechanisms under study. Finally, since photoexcitation and T_1 reductive quenching are common to both pathways, we have srutinized the photophysical properties of the $[(en)M(CO)_3Cl]$ complexes along with their T_1 excited states reduction potentials, $E^{\circ*}_{red}$. The $[(en)M(CO)_3Cl]$ complexes absorb mainly in the UV region while the absolute $E^{\circ*}_{red}$ are in the range 6.4–0.9 eV.

1. Introduction

The burning of fossil fuels is the main source of carbon dioxide, CO_2 released into the atmosphere by anthropogenic activity. Eighty per cent, 80% of the concentration of greenhouse gasses in the atmosphere is due to the human factor and more specifically to combustion for energy production. The energy sector, is to a large extent, based on the direct combustion of fuels, a process that in turn leads to large CO_2 emissions.[1] Carbon dioxide is one of the most important greenhouse gasses that contributes to the strengthening of this phenomenon on our planet. The main greenhouse gases are the following: carbon dioxide (CO_2), water vapor (H_2O), methane (CH_4), ozone (O_3), nitrogen dioxide (N_2O) and chlorofluorocarbons (CFC). Of these greenhouse gases, especially water vapor and carbon dioxide play a decisive role in regulating the temperature of the earth's surface and its atmosphere.[2] Many studies have been devoted to the way in which the problem of the continuous increase in atmospheric CO_2 can be resolved while at the same time there are continuous efforts and studies not only to bind CO_2 but at the same time to convert it into "fine chemicals".[3]

Among various strategies to achieve this goal, the biggest and most attractive challenge is the efficient conversion of CO_2 into useful compounds using sunlight as an energy source.[4] Many complexes with a transition metal element as metal center (such as Ni, Fe, Re, Cr, Ir, Mo *etc.*) have been extensively studied for the homogeneous electrocatalytic and photocatalytic reduction of carbon dioxide.[5–16]

The majority of research has focused on the photocatalytic reduction of CO_2, which has been based on systems that include a light unit consisting of a photosensitizer, (PS) and

Laboratory of Inorganic Chemistry, Department of Chemistry, University of Ioannina, 45110, Greece. E-mail: attsipis@uoi.gr

†Electronic supplementary information (ESI) available: 3D surfaces of the MOs involved in the most relevant electronic excitations in the simulated absorption spectra, Selected structural parameters of the various intermediates involved in step B of the catalytic cycle for the CO_2 to CO conversion, Gibbs free energies, *G* for all species involved in the Born–Haber cycle for redox potentials, parameters relevant to redox potentials, Cartesian coordinates and energetic data. See DOI: https://doi.org/10.1039/d4dt00125g

two catalytic sites (a reduction site and an oxidation site) (Scheme 1).[7–10,13–16]

At the oxidation site the donor provides an e^- to the PS after its excitation to the triplet excited state (^{3}MLCT) which is then reductively quenched at the reduction site and finally an e^- is transferred to CO_2. In many cases, however, PS acts not only as a PS but also as a reducing agent.[17]

So far, the majority of research efforts on the electro/photo-catalytic reduction of CO_2, has been put on 4d and 5d transition metal polypyridyl complexes as catalysts.[13] Among them, Re and Ru polypyridyl complexes have attracted the major concern, being the subject of numerous studies. In pioneering works,[18–20] Lehn *et al.*, studied the electro/photo-catalytic reduction of CO_2 to CO by Re(I) and Ru(II) bipyridyl complexes. Although, numerous mechanisms have been proposed for the photochemical reduction of CO_2 catalyzed by Re(I) and Ru(II) complexes, none of them could be regarded as universal.[16] Among the various mechanisms proposed, the most widespread is based on the formation of either $[Re(bpy)(CO)_3]$ or $[Re(bpy)(CO)_3]^{\bullet-}$ very reactive, five-coordinated key intermediates, able to capture CO_2.[21,22] Another proposed mechanism, based upon experimental[23] as well as theoretical[24] studies, involves the formation of a Re(I) dimer species *i.e.* $[Re(dmb)(CO)_3]_2(OCO)$, (dmb = 4,4′-dimethyl-2,2′-bipyridine) intermediate. In this dimeric Re(I) complex, from which CO is released, the CO_2 molecule bridges the two metal centres. Notice however, that the theoretical study[24] points out that formation of the Re(I) dimer is entropically unfavourable, while experiment[23] showed that this process is relatively slow. Nevertheless, the mechanism of CO_2 to CO reductions by Re(I) still remains elusive, especially the CO_2 addition to the metal centre.[16] Ishitani *et al.*,[23] proposed that even the non-reduced $[Re^I(N^N)(CO)_3]^+$ 17e$^-$ species is able to capture CO_2 with the assistance of TEOA. Accordingly, they found that during the photocatalytic reduction of CO_2 by the *fac*-$[Re^I(bpy)(Br)]$ complex, TEOA is coordinated to the metal centre of the non-reduced $[Re^I(bpy)(CO)_3]^+$ 17e$^-$ intermediate forming another intermediate namely the *fac*-$[Re^I(bpy)(CO)_3(OCH_2CH_2NR_2)]$ (R = CH_2CH_2OH). In a subsequent step, CO_2 is inserted into the Re–O coordination bond of the *fac*-$[Re^I(bpy)(CO)_3(OCH_2CH_2NR_2)]$ intermediate yielding the *fac*-$[Re^I(bpy)(CO)_3(R_2NCH_2CH_2O\text{-}COO)]$ insertion product, which is proposed to be the key intermediate for the CO_2 photocatalytic reduction.[23]

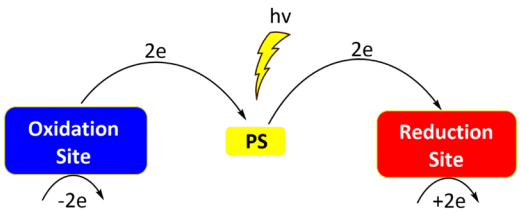

Scheme 1 Photocatalytic CO_2 reduction by a system comprising a PS and two catalytic sites.

The other most studied catalysts for electro/photo-catalytic CO_2 conversion are the Ru(II) polypyridyl complexes. The light-induced reduction of CO_2 to CO in an acetonitrile/water/triethanolamine solution in the presence of the $[Ru(2,2'\text{-bipyridine})_3]^{2+}/Co^{2+}$ system was first reported by Lehn and Ziessel.[18] Since then, numerous studies have been devoted to the CO_2 reduction by Ru(II) catalysts. The most representative complexes studied are the *cis*-$[Ru(bpy)_2(CO)X]^{n+}$, $[Ru(tpy)(bpy)X]^{n+}$ and *trans* (Cl)-$Ru(bpy)(CO)_2Cl_2$ complexes as well as their derivatives.[16]

The earliest study of electrochemical CO_2 reduction by a Ru(II) complex was reported by Tanaka *et al.*,[25] which used a homogeneous $[Ru(bpy)_2(CO)_2]^{2+}$ catalytic system to obtain a mixture of CO/formate from CO_2 upon electrolysis. The proposed mechanism, involves formation of an unsaturated five coordinate species which after reduction is attacked by CO_2 to form the $[Ru(bpy)_2(CO)(\eta^1\text{-}CO_2)]$ intermediate (η^1-CO_2 adduct). Formation of the η^1-CO_2 adduct is thought to occur also in the CO_2 electrocatalytic reduction by the *cis*-$[Ru(bpy)_2(CO)Cl]^+$ catalysts, which after reduction, loses the chloride ligand forming the unsaturated five coordinate species which in turn is attacked by CO_2.[26] An alternate combined η^1-CO_2 complex/CO_2 insertion (hydride) mechanism for CO_2 reduction has been proposed for Ru(II)-hydride catalysts.[16,27–29] Finally, Os(II) complexes are far less studied either as photosensitizers[30,31] or catalysts[32,33] for CO_2 conversion.

Taking into account the scarcity of theoretical studies of CO_2 to CO photocatalytic conversion by Ru or Os complexes we instigated to contact a theoretical study, by means of DFT/TDDFT electronic structure calculations, in order to delineate the mechanistic details of the CO_2 to CO photocatalytic conversion by simple Ru(II) and Os(II) octahedral model complexes of the general formula $[(en)M(CO)_3Cl]$ (en = ethylenediamine, M = Ru, Os) in the presence of TEOA. The aim of our work is twofold: (a) to expand our previous molecular modeling, mechanistic investigation on the photocatalytic CO_2 to CO reduction by Re(I) complexes[17] to cover also Ru(II) and Os(II) analogue complexes and (b) to theoretically delineate the possibility for the mechanism proposed by Ishitani's seminal work[23] on similar Re(I) bipy octahedral complexes to be valid also for Ru(II)/Os(II) complexes. Solvent effects on the reaction mechanisms of the CO_2 to CO conversion by $[(en)M(CO)_3Cl]$ complexes, were also studied, upon conducting our calculations in the non polar DCM solvent as well as in the polar DMF solvent. Finally, we set out to explore the photophysical properties of these complexes as well as their excited state electrochemistry.

2. Computational details

The geometries of all species have been fully optimized, without symmetry constraints, using the 1997 hybrid functional of Perdew, Burke and Ernzerhof[34–39] as implemented in the program Gaussian16.[40] This functional uses 25% exchange and 75% weighting correlation and is denoted as PBE0. The

Def2-TZVP basis set for all atoms was used for the geometry optimizations. The method used in the DFT calculations will be abbreviated PBE0/Def2-TZVP. All stable structures have been identified as energy minima with number of imaginary frequencies N_{Imag} = 0. In detail, the frequencies were calculated at the same level as in theory, and the nature of the fixed points was determined in each case according to the number of negative eigenvalues of the Hessian. The Gibbs free energy was calculated to be 298.15 K and 1 atm pressure. Solvent effects were calculated *via* the Polarizable Continuum Model (PCM) using the integral equation formalism variant (IEF-PCM), which is the default method (self-consistent reaction field (SCRF)).[41] DCM and the more polar solvent DMF were used as solvents. Natural Bond Orbital (NBO) population analysis was performed using the Weinhold methodology.[42,43] Time-dependent density functional theory (TD-DFT) calculations[44–47] were performed on the ground-state, S_0 equilibrium geometries in DCM and DMF solvents using the PBE0/Def2-TZVP/PCM computational protocol, taking account the first 30 excited states.

3. Results and discussion

Based upon previous experimental as well as theoretical evidences[16] we employed DFT electronic structure calculations in order to explore two possible reaction mechanisms for the photocatalytic CO_2 conversion by [(en)M(CO)$_3$Cl] octahedral complexes. The two possible mechanisms under investigation are: (a) The CO_2 to CO conversion, based on experimental studies by Ishitani *et al.*,[23] on Re(I) analogue complexes, where TEOA is thought to act, not only as a 'sacrificial donor', but also as a ligand as well, coordinated to the metal center of the 17e$^-$ very reactive intermediate and (b) a more conventional mechanism where the 17e$^-$ intermediate, after reduction, captures directly CO_2, to form the [(en)M(CO)$_3$(η^1-CO$_2$)] intermediate (η^1-CO$_2$ adduct).[16] Let us start however, with the computational study of the initial step of the reaction, being common to both possible reaction mechanisms under consideration, namely the photo-excitation and subsequent reductive quenching processes of the starting photocatalyst (or pre-catalyst).

3.1 Initial step

The initial step of the photocatalytic CO_2 to CO conversion by the [(en)M(CO)$_3$Cl] complexes, is depicted schematically in Fig. 1.

In the initial step, the [(en)M(CO)$_3$Cl] complexes, upon irradiation, are excited in their first singlet excited state, S_1 which *via* Intersystem Crossing (ISC) yields their first triple excited states, T_1. Finally, the [(en)M(CO)$_3$Cl] complexes in their T_1 state, receive an e$^-$ from TEOA forming the so called One Electron Reduced (OER), 19e$^-$ complex, **OER_M**.

The optimized geometries of all species in DCM, involved in the initial step of the CO_2 → CO conversion by [(en)Ru(CO)$_3$Cl], **1** and [(en)Os(CO)$_3$Cl], **2** complexes are depicted in Fig. 2 while those in DMF are given in Fig. S1 (see ESI).†

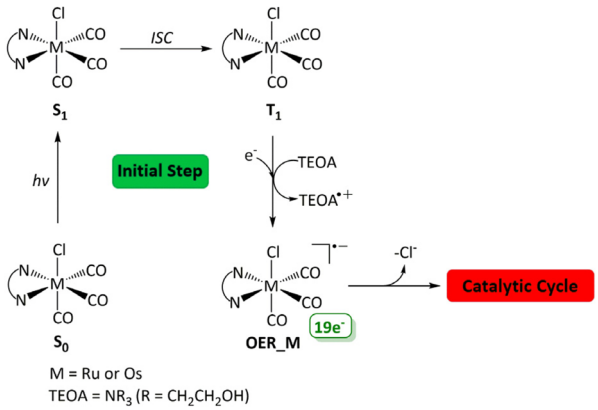

Fig. 1 Initial step of the photocatalytic CO_2 to CO conversion by the [(en)M(CO)$_3$Cl] complexes.

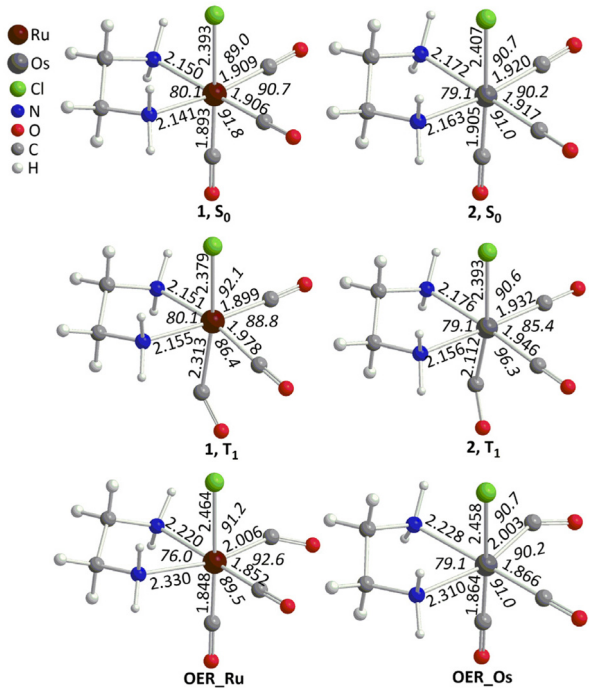

Fig. 2 Optimized geometries of **1** and **2** in their S_0 and T_1 states and respective OER species in DCM solvent at the PBE0/Def2-TZVP level.

Perusal of Fig. 2 and ES1† reveals that the structural parameters of **1** and **2** in their S_0 ground states are not affected and practically remain the same in either the non polar DCM solvent or in the polar DMF solvent. The same holds true also for **1** and **2** in their T_1 states. Upon S_0 → T_1 excitation, the most striking structural change is observed for the axial CO ligand *i.e.* the Ru–CO bond is significantly elongated by 0.2–0.4 Å while the ∠Ru–C–O bond angle departs from linearity by up to 47°. Also, there is a small change of the Ru–CO bonds of the equatorial CO ligands in the range 0.01–0.07 Å while the ∠CO$_{ax}$–Ru–CO$_{ax}$ and ∠CO$_{ax}$–Ru–CO$_{eq}$ bond angles change is in the range 1.9–5.4°. The rest of the structural para-

meters around the coordination sphere exhibit only minor changes.

On the other hand, the optimized geometry of the **OER_M** species in the two solvents, DCM and DMF remains practically unaltered. However, the structural parameters in the coordination sphere of **OER_M** species are significantly changed as compared to those found for the respective S_0 and T_1 states. Accordingly, the Ru–Cl bond in **OER_M** is elongated as compared to the respective bond in the S_0 and T_1 states. The same holds also for the two Ru–N bonds formed between the metal centers and the en ligand. In contrast, one Ru–CO_{eq} equatorial bond in **OER_M** is lengthen as compared to both the S_0 and T_1 states. This equatorial CO_{eq} ligand is also found to be significantly bended compared to S_0 and T_1 states. The other Ru–CO_{eq} equatorial bond in **OER_M** is shortened while retaining linearity. Finally, the Ru–CO_{ax} axial bond in **OER_M** is similar to that of S_0 state while both differ significantly compared to that in T_1 state. The bond angles around the coordination sphere in **OER_M** are similar to those found for the S_0 rather the T_1 state.

3.1.1 Photophysical properties. Since excitation of the initial photocatalyst/precatalyst, upon light irradiation, is a prerequisite in order to obtain the 17e$^-$ catalytically active intermediate, we set out to calculate the respective absorption spectra. In Fig. 3 are depicted schematically the simulated absorption spectraof **1** and **2** in both DCM and DMF solvents.

In Table 1 are given the respective electronic transitions related to the simulated absorption spectra of **1** and **2**. Inspection of Fig. 3 and Table 1 reveals that the two complexes in either DCM or DMF solvents, absorb in the UV region. Upon replacing the non-polar DCM solvent with the polar DMF solvent, has practically no effect on the absorption spectra which remain unaltered. The absorption spectra of **1**, in either DCM or DMF solvents, exhibit one band with peak around 180 nm and a shoulder at around 250 nm. The band arises mainly from an electronic excitation at 179 nm which based upon the shapes of the MOs involved in the respective electronic excitation (Fig. S2†), could be assigned as MLCT/MC/IL. The same holds also true for the shoulder peaking around 250 nm.

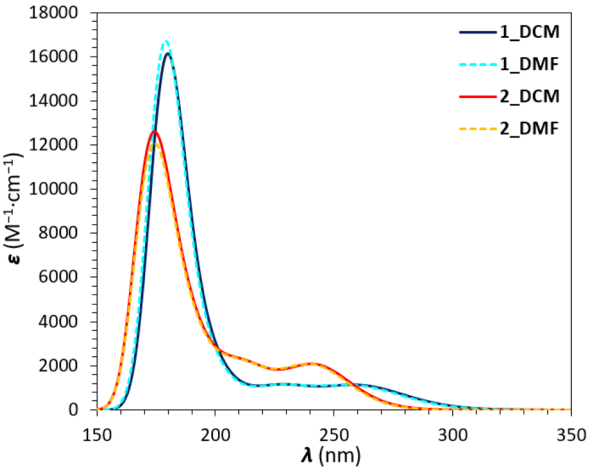

Fig. 3 Simulated absorption spectra of **1** and **2** in DCM and DMF solvents at the PBE0/Def2-TZVP level.

Table 1 Principal singlet–singlet electronic transitions in the simulated absorption spectra, for **1** and **2** calculated in DCM and DMF solvents at the PBE0-GD3BJ/Def2-TZVP level of theory

Excitation (%composition)	E (eV)	λ (nm)	f
1_DCM			
H−5 → L (32%), H−3 → L (23%), H−3 → L+2 (11%)	6.92	179	0.354
H−1 → L+1 (70%)	4.83	257	0.015
1_DMF			
H−5 → L (43%), H−3 → L (15%)	6.96	178	0.373
H−1 → L+1 (73%)	4.86	255	0.014
2_DCM			
H−4 → L+2 (12%), H−3 → L+2 (30%), H−2 → L+7 (13%)	7.32	169	0.060
H−5 → L+1 (15%), H−2 → L+6 (48%)	7.25	171	0.081
H−2 → L+4 (25%), H−2 → L+5 (10%), H−2 → L+6 (25%)	7.16	173	0.074
H−1 → L+7 (19%), H → L+7 (20%)	6.94	179	0.110
H−1 → L+2 (57%), H → L+2 (18%)	5.83	213	0.014
H−2 → L (36%), H−2 → L+1 (36%)	5.79	214	0.020
H−1 → L+1 (53%), H → L (30%)	5.13	242	0.043
2_DMF			
H−4 → L+2 (15%), H−3 → L+2 (36%)	7.33	169	0.057
H−5 → L (12%), H−2 → L+6 (43%)	7.26	171	0.067
H−2 → L+4 (−23%), H−2 → L+6 (33%)	7.17	173	0.064
H−1 → L+7 (17%), H → L+7 (20%)	6.97	178	0.113
H−2 → L (14%), H−2 → L+1 (57%)	5.79	214	0.020
H−1 → L+1 (54%), H → L (22%)	5.16	240	0.042

The simulated absorption spectra of **2** in DCM and DMF solvents exhibit one high energy strong band, peaking around 170 nm and a lower energy, weak band at around 240 nm. In addition, there is a shoulder around 215 nm. Based upon the shapes of the MOs involved in the electronic excitations (Fig. S2†) the bands and the shoulder are assigned as MLCT/MC/IL.

Since the T_1 excited states of the complexes under study is of central importance in Step A, we set out to explore their properties in more detail. In Fig. 4 are depicted the spin density along with the SOMOs for the T_1 excited state of **1** and **2**.

Inspection of Fig. 4 reveals that the spin density in the T_1 state of **1** and **2** is mainly accumulated on the metal center and to a lesser degree on the axial chloride and carbonyl ligands. The spin density distribution resembles the 3D shapes of the SOMOs of **1** and **2** in the T_1 state.

3.1.2 Excited state redox potentials. Taken into account that formation of the 17e$^-$ catalytically active intermediate is preceded by the reductive quenching of the first triplet excited state, T_1 of the pre-catalyst, we set out to calculate the redox potential for this excited state. The T_1 excited-state redox potentials were estimated upon employing the procedure followed by Hansen *et al.*[48] First, we calculated the ground-state reduction potentials, E°_{red} based upon the Born–Haber cycle shown in Scheme 2. Then, we calculated the excited state

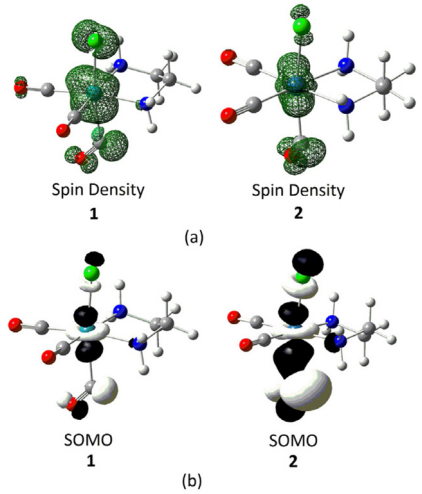

Fig. 4 (a) Spin density isosurfaces (0.005 au) along with atomic spin densities of T_1 state of complexes **1** and **2** in DCM solvent (numbers in parenthesis refer to DMF solvent) and (b) 3D contour plots of the relevant SOMOs at the PBE0-GD3BJ/Def2-TZVP level of theory.

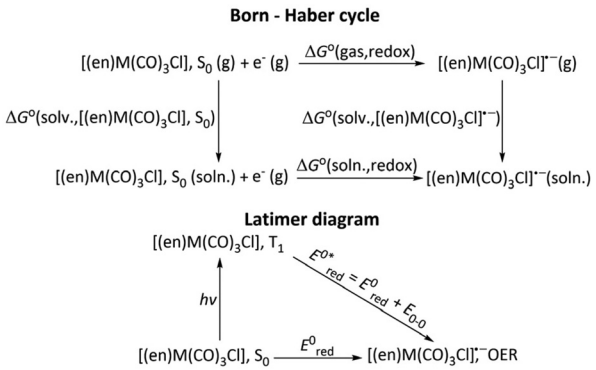

Scheme 2 Born–Haber cycle employed in the calculation of the ground state reduction potentials, E°_{red} (above) and Latimer diagram employed for the calculation of T_1 excited state reduction potentials, $E^{\circ *}_{red}$ (below).

reduction potential, $E^{\circ *}_{red}$ according to the Latimer diagram depicted also in Scheme 2.

The standard absolute ground-state reduction potential, E°_{red} is calculated by the following equation:

$$E^{\circ}_{red} = -\Delta G^{\circ}(\text{soln. redox})/ZF \quad (1)$$

where F is the Faraday constant (23.061 kcal per volt gram equivalent) and Z is unity for one-electron redox processes. ΔG°(soln., redox) is obtained from the following equation:

$$\Delta G^{\circ}(\text{soln., redox}) = \Delta G^{\circ}(\text{gas, redox}) + \Delta G^{\circ}(\text{solv., } [(\text{en})\text{M}(\text{CO})_3\text{Cl}]^{\bullet -}) - \Delta G^{\circ}(\text{solv., } [(\text{en})\text{M}(\text{CO})_3\text{Cl}], \text{S}_0). \quad (2)$$

The calculated Gibbs free energies appearing in Scheme 2 are given in Tables S1 and S2 of the ESI† along with 0–0 transition energies for the T_1 states, E_{0-0} in DCM and DMF solvents. The E_{0-0} are obtained as the differences of the zero point energy corrected total electronic energies of **1** and **2** in their S_0 and T_1 states in DCM and DMF solvents. The calculated T_1 excited state absolute reduction potentials, $E^{\circ *}_{red}$ are 6.4 and 6.3 V for **1** in DCM and DMF respectively, while for **2** are 6.4 and 0.9 V in DCM and DMF respectively. Taking into account that SHE potential is −4.281 V,[49] the $E^{\circ *}_{red}$ *vs.* SHE for **1** in DCM and DMF are 2.1 and 2.0 Volt respectively while for **2** in DCM and DMF are 2.0 and −3.4 V.

3.2 Catalytic cycle

After the photoexcitation and reductive quenching processes in the Initial step of the photocatalytic CO_2 to CO conversion, it follows the 'actual' catalytic cycle, starting with the five coordinated, 17e$^-$ intermediate. We examined two possible mechanisms for the catalytic cycle. The first possible mechanism is based on the concept of the formation of a complex between the 17e$^-$ catalytically active intermediate and TEOA, acting as a ligand. Henceforth, we will call this the TEOA complex mechanism. The second possible mechanism under investigation, is based on the direct CO_2 capture by the 17e$^-$ catalytically active intermediate which henceforth we will call it η^1-CO_2 complex mechanism.

3.2.1 TEOA complex mechanism. This proposed mechanism is based on the formation of a complex between TEOA and the 17e$^-$ five coordinated intermediate obtained from **OER_M**. This concept is thought[23,50] to be important for the CO_2 reduction in low concentrations *e.g.* in the air, and its utilization from dilute CO_2 sources. However, obtaining CO *via* this mechanism still remains elusive. Accordingly, we employed DFT electronic structure calculations to study in more depth the concept of the TEOA complex mechanism applying it for the Ru(II) and Os(II) catalysts under consideration. The proposed catalytic cycle is depicted in Fig. 5 and comprising two steps: (a) the TEOA complex formation step and (b) the CO release step.

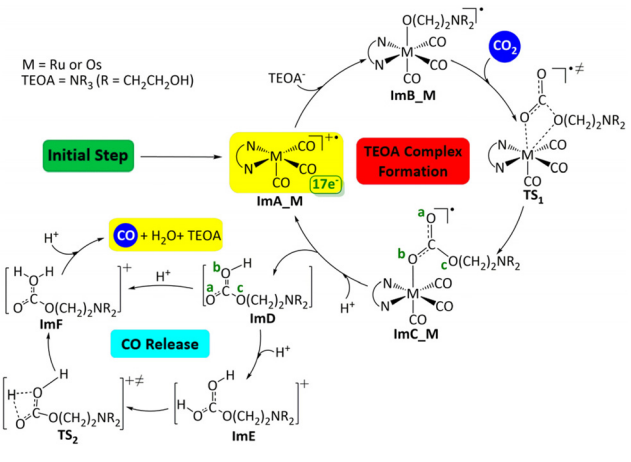

Fig. 5 Proposed TEOA complex mechanism for CO_2 to CO conversion by **1** and **2**.

3.2.1.1 TEOA complex formation step. The TEOA complex formation step starts with the 17e$^-$ five coordinated, very reactive intermediates, **ImA_M**, obtained from **OER_M**, and considered to be the 'true' catalysts. Next, TEOA upon deprotonation, is coordinated, as an anionic ligand, TEOA$^-$, to the metal center of **ImA_M**, forming the [(en)(CO)$_3$M(OCH$_2$CH$_2$NR$_2$)] intermediates, **ImB_M**. The CO_2 molecule could then be captured *via* an insertion reaction, where it is inserted into the M–O bond of **ImB_M** yielding the [(en)(CO)$_3$MO(O)COCH$_2$CH$_2$NR$_2$] key intermediates, **ImC_M** which are of significant importance.[23] The latter, upon protonation, dissociate to form the [R$_2$NCH$_2$CH$_2$OC(O)OH]$^+$ species, **ImD_M** and giving back the 'true' catalysts, **ImA_M**. The free energy, ΔG profiles calculated for the TEOA complex formation cycle are depicted schematically in Fig. 6 and 7 for the Ru(II) complex **1** and Os(II) complex **2** respectively, in both DCM and DMF solvents.

Notice that, in the mechanistic profiles depicted in Fig. 6 and 7, the 'magic' TEOA sacrificial electron donor is thought of acting as the proton donor as well. Perusal of Fig. 6 and 7 reveals that the TEOA complex formation step is expected to be endergonic in the case where TEOA is thought to be the proton donor source. Initially, coordination of TEOA$^-$ ligand to the metal center of either **ImA_Ru** or **ImA_Os** is exergonic in either DCM or DMF solvents. This process is slightly more favorable for Os(II) complex, **2** as compared to the Ru(II) complex, **1**. In addition, the TEOA$^-$ coordination to the metal centers is clearly more favorable in DCM rather in DMF solvent. Next, the CO_2 insertion into the M–O bond of **ImB_M** species proceeds *via* a transition state, **TS$_1$_M**, leading to intermediate **ImC_M** (Fig. 6 and 7). The calculated energy barrier for the formation of **ImC_M** from **ImB_M** is estimated to be in the range 36–42 kcal mol^{-1} at the PBE0/Def2-TZVP level of theory. It should be noticed that, this process is slightly more favorable for Ru(II) complex, **1** rather for Os(II) complex, **2**, since the energy barrier for the former is lower than for the latter. Finally, upon protonation of **ImC_M**, with TEOA as the proton source, we obtain the **ImD** intermediate and **ImA_M** *via* a somewhat endergonic process.

Taking into account that for similar Re(I) complexes the proton obtained from the deprotonated form of TEOA should be trapped by another TEOA molecule[23] we set out to explore this possibility also for the Ru(II) and Os(II) complexes under study. Inspection of Fig. 6 and 7 reveals that protonation with TEOA(H)$^+$, as the proton source, is exergonic in contrast to the process where TEOA is used as a proton source.

The relatively weak Ru–O coordination bond, formed upon coordination of the R$_2$NCH$_2$CH$_2$O$^-$ (R = CH$_2$CH$_2$OH) ligand to the Ru metal center of the [(en)Ru(CO)$_3$] intermediate, **ImA_Ru**, is reflected to the relatively small Wiberg Bond Indices (WBI) obtained from the NBO analysis of **ImB_Ru**, being equal to 0.582 and 0.581 in DCM and DMF solvents respectively.

In addition, NBO population analysis revealed that in DCM and DMF solvents both the Ru metal center and the O donor atom of the R$_2$NCH$_2$CH$_2$O$^-$ ligand acquire negative natural atomic charges equal to −0.850 and −0.707|*e*| respectively, resulting in a repulsive electrostatic interaction. On the other hand, in both DCM and DMF solvents, the covalent component of the Ru–O coordination bond arises from a σ(Ru–O) bonding NBO, formed upon interaction of the sp$^{4.90}$d$^{4.24}$ hybrid orbitals (48.3% p and 41.7% d character) of Ru with the sp$^{2.60}$ hybrid orbital (72.2% p-character) of the oxygen donor atom of R$_2$NCH$_2$CH$_2$O$^-$ ligand and is described as σ(Ru–O) = 0.429h_{Ru} + 0.903h_O. The occupation number of σ(Ru–O) NBO

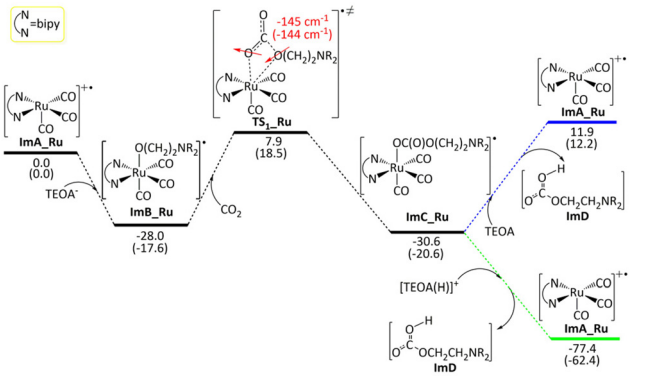

Fig. 6 Free energy, ΔG (in kcal mol^{-1}), reaction profiles of TEOA complex cycle for **1** in DCM and DMF (numbers in parenthesis) solvents calculated at the PBE0/Def2-TZVP level.

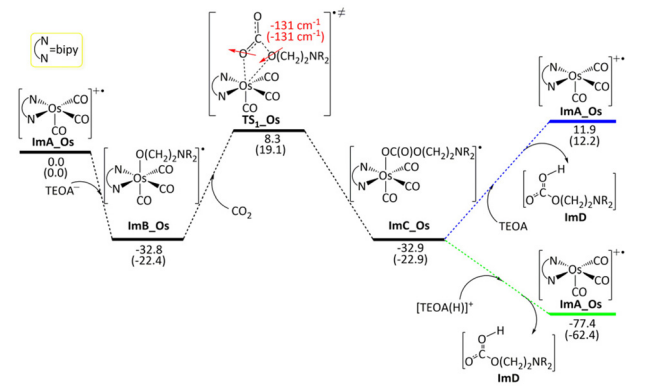

Fig. 7 Free energy, ΔG (in kcal mol^{-1}), reaction profiles of TEOA complex cycle for **1** in DCM and DMF (numbers in parenthesis) solvents calculated at the PBE0/Def2-TZVP level.

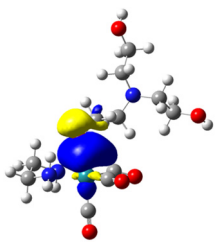

Scheme 3 3D surface of the σ(Ru–O) bonding NBO of **ImB_Ru**.

is 0.958|*e*|. The σ(Ru–O) NBO is depicted schematically in Scheme 3.

It follows the insertion of a CO_2 molecule into the Ru–O bond of **ImB_Ru** yielding **ImC_Ru** *via* an exergonic process with ΔG equal to −31 to −21 kcal mol^{-1} in DCM and DMF solvents respectively. Formation of **ImC_Ru** procceds *via* transition state **TS$_1$_Ru**, exhibiting a relatively low energy activation barrier calculated to be 8 and 19 kcal mol^{-1} in DCM and DMF solvents respectively (Fig. 6). Subsequently, **ImC_Ru** could undergo protonation at three possible O atom sites of the $R_2NCH_2CH_2O(O)CO$ ligand denoted as O_a, O_b and O_c (Fig. 5). The natural atomic charges on the O_a and O_b atoms are −0.719 and −0.649 respectively in DCM solvent and −0.724 and −0.648 respectively in DMF solvent. Protonation of either O_a or O_b of the $R_2NCH_2CH_2OC(O)O$ ligand leads to cleavage of the Ru–O bond, yielding **ImD** and regenerating the initial 17e$^-$ catalytic species **ImA_Ru**, thus closing the catalytic cycle (Fig. 5).

The third possible protonation site *i.e.* O_c acquires a natural atomic charge of only −0.519, thus being less prone to protonation as compared to the other two possible protonation sites, O_a and O_b of **ImC_Ru**. However, the protonation of the third possible site, O_c yields back **ImA_Ru**, CO_2 and TEOA.

Protonation of **ImC_Ru**, with TEOA proton donor, at O_a and O_b sites, leading to Ru–O bond cleavage to yield **ImA_Ru** and **ImD**, is estimated to be a slightly endergonic process with ΔG around to 12 kcal mol^{-1} in both DCM and DMF solvents respectively (Fig. 6). In contrast, if TEOA(H)$^+$ is the proton donor, this process is exergonic with ΔG equal to 77 and 62 kcal mol^{-1} in DCM and DMF solvents respectively.

The calculated free energy reaction profile for **2** is quite similar with that calculated for **1** (Fig. 7). The anionic TEOA$^-$ ligand interacts with the Os metal center of the highly active 17e$^-$ intermediate **ImA_Os**, giving the neutral radical [(en)Os(CO)$_3$(TEOA)]$^\bullet$ intermediate, **ImB_Os**. The estimated interaction energy (IE) of TEOA$^-$ ligand with the Os metal center of **ImB_Os** is equal to −44.6 kcal mol^{-1} in DCM solvent and −34.3 kcal mol^{-1} in DMF solvent.

Obviously, TEOA$^-$ interacts more strongly with Os rather than the Ru metal center of **ImA_M**. The conversion of **ImA_Os** to the **ImB_Os** intermediate is slightly more exergonic (ΔG = −33 and −22 kcal mol^{-1} in DCM and DMF solvents respectively) as compared to the respective process calculated for the Ru counterparts.

NBO analysis indicates that the TEOA$^-$ ligand coordinates to the Os metal center of **ImA_Os**, forming a relatively weak Os–O bond in the **ImB_Os** intermediate. The estimated WBI for Os–O bond is 0.528 in DCM solvent and 0.529 in DMF solvent. In DCM solvent both the Os metal center and the O donor atom of the coordinated TEOA$^-$ ligand acquire negative natural atomic charges of −0.397 and −0.761|*e*| respectively. In DMF solvent, the respective charges are −0.400 and −0.757|*e*| respectively. The electrostatic interaction between TEOA$^-$ ligand with Os metal center of **ImB_Os** is unfavorable similar to that found for the respective Ru intermediate, **ImB_Ru**.

Formation of **ImC_Os** for **2** *i.e.* CO_2 insertion into the Os–O (TEOA) bond is calculated to be slightly more exergonic as compared to its Ru counterpart (Fig. 6 and 7). It follows protonation of **ImC_Os** at either O_a or O_b sites leading ultimately to the formation of **ImA_Os** and **ImE** intermediates (Fig. 7). The protonation sites O_a and O_b acquire natural atomic charges of −0.712 and −0.728|*e*| respectively in DCM solvent and −0.728 and −0.697|*e*| respectively in DMF solvent. Protonation of **ImC_Os**, with TEOA, accompanied by the cleavage of the Ru–O bond, is slightly endergonic, similar to that found for the protonation of the respective Ru intermediate, **ImC_Ru**. In contrast, protonation with TEOA(H)$^+$ is exergonic just as for its Ru counterpart.

Notice that, as in the case of **1**, there is a third protonation site at O_c (Fig. 5) being less probable however, due to the lower negative natural charge calculated for O_c, being equal to −0.516 and −0.508|*e*| in DCM and DMF solvents respectively. The protonation of the third possible site, O_c yields back **ImA_Os**, CO_2 and TEOA similar with the respective process being observed for **1** (*vide supra*). Finally, the optimized geometries of all species involved in the catalytic cycle of TEOA complex formation step (Fig. 5) along with selected structural parameters are given in Fig. S3 and S4 of the ESI.†

3.2.1.2 CO release step. The second step of the TEOA complex mechanism, starts with the $[R_2NCH_2CH_2OC(O)OH]^+$ species, **ImD**, being the product of protonation of **ImC_M** during the preceding TEOA complex formation step (Fig. 5). The energetic profile calculated for the CO release step is depicted in Fig. 8. As for the TEOA complex formation step (*vide supra*), we examined two possible reaction mechanisms *i.e.* one where TEOA acts as the proton source and another where protonated TEOA, TEOA(H)$^+$ is the proton source. There are three possible protonation sites in **ImD** which are denoted as O_a, O_b and O_c (Fig. 8). The natural atomic charges of the O_a, O_b and O_c atoms of **ImD** in DCM are −0.644, −0.680 and

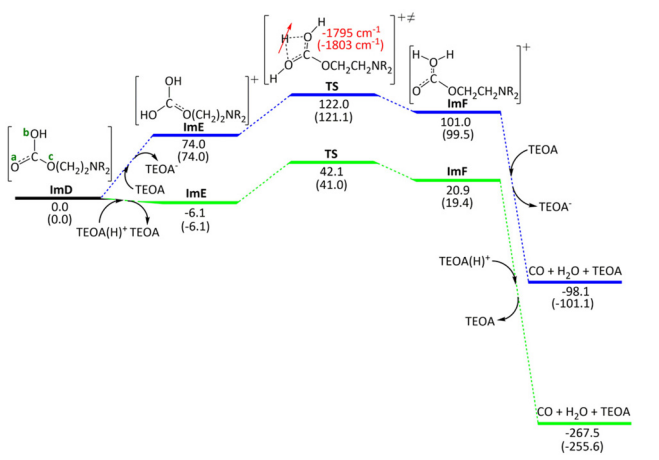

Fig. 8 Free energy, ΔG (in kcal mol^{-1}), reaction profiles for CO release step in DCM and DMF (numbers in parenthesis) solvents, with TEOA and TEOA(H)$^+$ as proton donors (blue and green lines respectively), calculated at the PBE0/Def2-TZVP level.

−0.476|*e*| respectively while in DMF are −0.648, −0.679 and −0.477|*e*| respectively. Thus, based upon the natural charges, the most probable protonation site is O_b followed by O_a and O_c. Protonation at O_b yields directly a protonated derivative of **ImD** namely intermediate **ImF**. The latter could also be formed, *via* a transition state **TS**, upon protonation at the second most probable site of **ImD** *i.e.* O_a (Fig. 8). Finally, protonation of **ImF** at site O_c (protonation at site O_a does not lead to products formation) yields CO and H_2O while regenerating TEOA.

It should be stressed here, that the most facile route to products formation in the TEOA complex formation step is expected to proceed *via* protonation of **ImD** at site O_b, with $TEOA(H)^+$ as the proton source since in this case direct formation of **ImF** exhibits a relatively low energy barrier around 20 kcal mol^{-1}. All the other paths examined *i.e.* protonation of **ImD** at either site O_b, with TEOA proton donor or at site O_a, with $TEOA/TEOA(H)^+$ proton donors exhibit very high energetic barriers rendering them unfavorable.

The TEOA complex formation step yielding CO, H_2O and regenerating TEOA is calculated to be strongly exergonic for all routes examined with ΔG ranging from −98 to −268 kcal mol^{-1}.

The optimized geometries of all species involved in the catalytic cycle of CO release step (Fig. 8) are given in Fig. S5 of the ESI.†

3.2.2 η^1-CO_2 complex mechanism. The second possible mechanism, examined for the CO_2 electro/photocatalytic conversion by Ru(II)/Os(II) complexes under study, is based on the direct CO_2 capture by the 17e$^-$ catalytically active intermediate. This mechanism is the most popular and widespread to people working in this area. The proposed catalytic cycle, involving the η^1-CO_2 complex formation, is depicted schematically in Fig. 9.

It can be seen that, in the η^1-CO_2 complex mechanism, the five coordinated, 17e$^-$ catalytically active intermediate, **ImA_M** is one electron reduced with TEOA to yield the five coordinated intermediate **ImB′_M**. This step has been proposed also to occur during the photocatalytic CO_2 to CO reduction by the *trans*-Ru(bpy)$(CO)_2Cl_2$ complex.[51] Next, CO_2 is captured by the reactive **ImB′_M** species forming the η^1-CO_2 complex, **ImC′_M** which is considered to be a key intermediate. The CO_2 capture/activation step proceeds *via* transition state **TS_1′_M**. The formation of **ImC′_M** is followed by two successive protonations of **ImC′_M** with TEOA acting as the proton source, yielding subsequently **ImD′_M** and **ImE′_M** intermediates (Fig. 9). The **ImE′_M** intermediate loses a water molecule, producing the tetracarbonyl intermediate, **ImF′_M**. This process proceeds *via* transition state **TS_2′_M**. Finally, **ImF′_M** receives an e$^-$ from TEOA forming the reduced **ImG′_M** intermediate which is then yields CO and the initial catalytic species **ImA_M**.

The optimized geometries of all the species participating in the catalytic cycles depicted in Fig. 9, along with selected structural parameters are given in Fig. S6 and S7† for Ru and Os species respectively in both DCM and DMF solvents. The calculated free energy, ΔG profiles for **1** and **2** in DCM and DMF solvents are given in Fig. 10 and 11 respectively. Inspection of Fig. 10 and 11 reveals that the one electron reduction of **ImA_M** with TEOA to yield **ImB′_M** is endergonic. Next, we have the formation of **ImC′_M** *via* transition state **TS_1′_M** with an energy barrier estimated to be in the range 48–50 kcal mol^{-1}. The protonation of **ImC′_M** to yield **ImD′_M** could proceed either with TEOA or with protonated $TEOA(H)^+$. However, protonation with the former is predicted to be unfavourable while for the latter it is favourable. Subsequent protonation of **ImD′_M**, with TEOA (blue lines, Fig. 10 and 11) to yield **ImE′_M** as well as formation of the tetracarbonyl intermediates, **ImF′_M** and **ImG′_M** *via* transition state **TS_2′_M** are

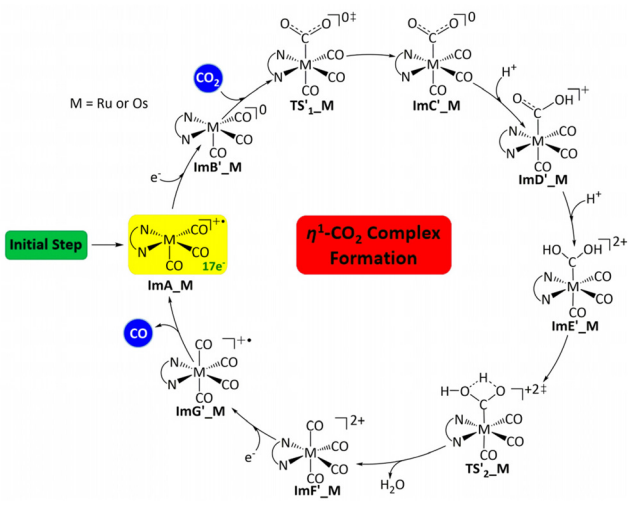

Fig. 9 Proposed η^1-CO_2 complex mechanism for CO_2 to CO conversion by **1** or **2**.

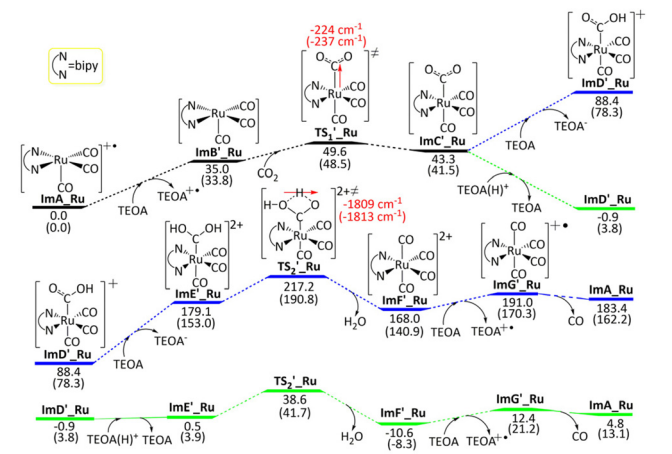

Fig. 10 Free energy, ΔG (in kcal mol^{-1}), reaction profile for the CO_2 to CO conversion by **1**, following the η^1-CO_2 complex mechanism, in DCM and DMF (numbers in parenthesis) solvents, with TEOA as proton donor (blue lines) and with $TEOA(H)^+$ (green lines), calculated at the PBE0/Def2-TZVP level.

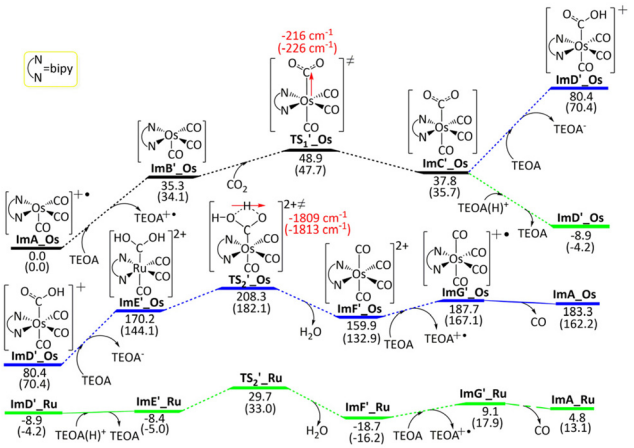

Fig. 11 Free energy, ΔG (in kcal mol^{-1}), reaction profile for the CO_2 to CO conversion by **2**, following the η^1-CO_2 complex mechanism, in DCM and DMF (numbers in parenthesis) solvents, with TEOA as proton donor (blue lines) and with TEOA(H)$^+$ (green lines), calculated at the PBE0/Def2-TZVP level.

expected to be highly unfavourable exhibiting quite high energy barriers. Finally, formation of CO giving back also the initial intermediate **ImA_M** is an endergonic process. In contrast to TEOA, the path with TEOA(H)$^+$ (green lines, Fig. 10 and 11) is expected to be more favourable.

Accordingly, protonation of **ImD′_M**, with TEOA(H)$^+$ is almost barrierless, while formation of the tetracarbonyl intermediates proceeds *via* **TS$_2$′_M** exhibiting a relatively low energy activation barrier. The path followed upon employing TEOA(H)$^+$ is predicted to be slightly endergonic.

Since **ImC′_M** is of key importance for CO_2 to CO conversion we set out to analyse in more depth the nature of the M–CO_2 bond by means of NBO analysis method. Thus, the natural charges on Ru and C atoms of the Ru–CO_2 bond in **ImC′_Ru** are equal to −1.307 and 0.794|*e*| in DCM and −1.302 and 0.790|*e*| in DMF solvent. On the other hand, the natural charges on Os and C atoms of the Os–CO_2 bond in **ImC′_Os** are equal to −0.817 and 0.685|*e*| in DCM and −0.813 and 0.682|*e*| in DMF solvent. Obviously, there is favourable electrostatic attraction between the constituent atoms of the M–CO_2 bond. In addition, the M–CO_2 bond is expected to have a small covalent component as well, since the WBIs are 0.660 and 0.671 for the Ru–CO_2 bond in DCM and DMF solvents respectively while the respective WBIs for the Os–CO_2 bond are 0.672 and 0.679. The covalent nature of the M–CO_2 is demonstrated also by the existence of a bonding NBO (Scheme 4).

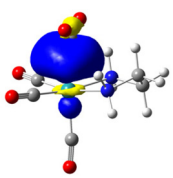

Scheme 4 3D surface of the σ(Ru–C) bonding NBO of **ImC_Ru**.

The above bonding NBO is formed upon interaction of the $sp^{3.28}d^{2.70}$ hybrid orbitals (47.0% p and 38.6% d character) of Ru with the $sp^{2.35}$ hybrid orbital (70.1% p-character) of the carbon atom of CO_2 and is described as σ(Ru–O) = $0.702h_{Ru}$ + $0.713h_C$. The occupation number of σ(Ru–C) NBO is 1.752|*e*|.

4. Conclusions

The photocatalytic CO_2 to CO reduction by [(en)M(CO)$_3$Cl], Ru(II) and Os(II) octahedral complexes was studied by means of DFT calculations. In an initial step, the [(en)M(CO)$_3$Cl] complexes, upon irradiation, are excited in their T_1 state which upon one electron reduction with TEOA, are converted to the OER species. It follows the main catalytic cycle which starts with a 17e$^-$ five coordinated species, obtained from OER upon losing its chloride ligand. Two possible mechanisms were examined for the main catalytic cycle: (a) the TEOA complex mechanism and (b) the η^1-CO_2 complex mechanism. At the beginning, we scrutinized the initial step of the photocatalytic process under study. The TDDFT simulated absorption spectra of the initial photocatalysts, [(en)M(CO)$_3$Cl] in DCM and DMF solvents, exhibit absorption bands mainly in the UV region. The polarity of the solvent does not affect the absorption spectra. In contrast, the calculated T_1 excited state reduction potentials, $E^{\bigcirc *}_{red}$ depend upon the solvent and reveal that **1** and **2** in DCM are the easiest to be reductively quenched.

The TEOA complex mechanism proposed for the main catalytic cycle, succeeding the Initial Step, is based on the formation of the complex [(en)M(CO)$_3$(OCH$_2$CH$_2$NR$_2$)] between the 17e$^-$ five coordinated catalytically active intermediate with TEOA$^-$ anion acting as O-donor ligand. A similar Re(I) complex as well as its CO_2 insertion product have already been experimentally observed.[23] The TEOA complex mechanism is thought to occur in two steps. In the first step, the catalytically active intermediate **Im_A** is regenerated and a metal 'free' intermediate, **Im_D** is also produced. The latter, starts the second step were *via* two possible pathways, produces CO, TEOA and H_2O. It is anticipated that the proton donor source should play a crucial role in the TEOA complex mechanism. Thus, if TEOA is the proton donor, the TEOA complex formation step is predicted to be slightly endergonic while if TEOA(H)$^+$ is the proton donor, this step is strongly exergonic. The CO release step is exergonic using either TEOA or TEOA(H)$^+$ proton donors. However, use of TEOA proton donor in the CO release step, results in very high activation energy barriers in contrast to TEOA(H)$^+$ proton donor where the activation energy barriers are much lower. Therefore, this step is expected to be kinetically more favorable if the proton source is TEOA(H)$^+$.

The η^1-CO_2 complex mechanism is based on earlier studies proposing a two electron – two proton process with TEOA acting as a sacrificial anode. This mechanism starts also with the 17e$^-$ catalytically active intermediate which upon one electron reduction, captures CO_2 and forming a loosely bound η^1-CO_2 complex. Successive protonations and one electron

reduction yields CO while regenerating the $17e^-$ catalytically active intermediate. The whole process is predicted to be endergonic though it has to surmount a significant activation barrier. The latter should be alleviated in the case of electrocatalytic CO_2 to CO reduction by the complexes under study. As is for the TEOA complex mechanism, the η^1-CO_2 complex mechanism is favored with $TEOA(H)^+$ proton donor.

The geometric and the energetic profiles of both mechanisms are not significantly affected by the nature of the solvent. We believe that, the TEOA complex mechanism should be of importance in low CO_2 concentrations[23] while the η^1-CO_2 complex mechanism is a more general approach for CO_2 to CO electrocatalytic/photocatalytic conversion.

Overall, the present theoretical study, being a follow up of our previous work on Re(I) complexes,[17] is an extension to cover also the photocatalytic CO_2 to CO conversion by similar Ru(II)/Os(II) simple model complexes, highlighting the role of the TEOA 'magic' sacrificial donor. Our molecular modeling works on Re(I), Ru(II) and Os(II) complexes proposes for the first time an alternative 'unconventional' mechanism which could trigger further experimental works aiming at fully delineating the photocatalytic CO_2 to CO reduction using TEOA.

Conflicts of interest

There are no conflicts to declare.

References

1 R. Quadrelli and S. Peterson, *Energy Policy*, 2007, **35**, 5938–5952.
2 B. J. Mason, *Contemp. Phys.*, 1989, **30**, 417–432.
3 M. Cokoja, C. Bruckmeier, B. Rieger, W. A. Herrmann and F. E. Kühn, *Angew. Chem., Int. Ed.*, 2011, **50**, 8510–8537.
4 A. J. Morris, G. J. Meyer and E. Fujita, *Acc. Chem. Res.*, 2009, **42**, 1983–1994.
5 J. A. Keith, K. A. Grice, C. P. Kubiak and E. A. Carter, *J. Am. Chem. Soc.*, 2013, **135**, 15823–15829.
6 C. Riplinger, M. D. Sampson, A. M. Ritzmann, C. P. Kubiak and E. A. Carter, *J. Am. Chem. Soc.*, 2014, **136**, 16285–16298.
7 H. Koizumi, H. Chiba, A. Sugihara, M. Iwamura, K. Nozaki and O. Ishitani, *Chem. Sci.*, 2019, **10**, 3080–3088.
8 Y. Asai, H. Katsuragi, K. Kita, T. Tsubomura and Y. Yamazaki, *Dalton Trans.*, 2020, **49**, 4277–4292.
9 I. Choudhuri and D. G. Truhlar, *J. Phys. Chem. C*, 2020, **124**, 8504–8513.
10 Y. S. Gong, J. Fan, V. Cecenc and C. Huang, *Chem. Eng. J.*, 2021, **405**, 12613–12627.
11 K. S. Rawat, A. Mahata, I. Choudhuri and B. Pathak, *J. Phys. Chem. C*, 2016, **120**, 8821–8831.
12 D. H. Apaydin, S. Schlager, E. Portenkirchner and N. S. Sariciftci, *ChemPhysChem*, 2017, **18**, 3094–3116.
13 N. Elgrishi, M. B. Chambers, X. Wang and M. Fontecave, *Chem. Soc. Rev.*, 2017, **46**, 761–796.
14 K. E. Dalle, J. Warnan, J. J. Leung, B. Reuillard, I. S. Karmel and E. Reisner, *Chem. Rev.*, 2019, **119**, 2752–2875.
15 Y. Yamazaki, H. Takeda and O. Ishitani, *J. Photochem. Photobiol., C*, 2015, **25**, 106–137.
16 Y. Kuramochi, O. Ishitani and H. Ishida, *Coord. Chem. Rev.*, 2018, **373**, 333–356.
17 A. C. Tsipis and A. A. Sarantou, *Dalton Trans.*, 2021, **50**, 14797–14809.
18 J.-M. Lehn and R. Ziessel, *Proc. Natl. Acad. Sci. U. S. A.*, 1982, **79**, 701–704.
19 J. Hawecker, J.-M. Lehn and R. Ziessel, *J. Chem. Soc., Chem. Commun.*, 1983, 536–538.
20 J. Hawecker, J.-M. Lehn and R. Ziessel, *Helv. Chim. Acta*, 1986, **69**, 1990–2012.
21 J. M. Smieja and C. P. Kubiak, *Inorg. Chem.*, 2010, **49**, 9283–9289.
22 H. Takeda, K. Koike, H. Inoue and O. Ishitani, *J. Am. Chem. Soc.*, 2008, **130**, 2023–2031.
23 T. Morimoto, T. Nakajima, S. Sawa, R. Nakanishi, D. Imori and O. Ishitani, *J. Am. Chem. Soc.*, 2013, **135**, 16825–16828.
24 J. Agarwal, E. Fujita, H. F. Schaefer and J. T. Muckerman, *J. Am. Chem. Soc.*, 2012, **134**, 5180–5186.
25 H. Ishida, K. Tanaka and T. Tanaka, *Chem. Lett.*, 1985, **14**, 405–406.
26 H. Ishida, K. Tanaka and T. Tanaka, *Organometallics*, 1987, **6**, 181–186.
27 P. Kang, C. Cheng, Z. Chen, C. K. Schauer, T. J. Meyer and M. Brookhart, *J. Am. Chem. Soc.*, 2012, **134**, 5500–5503.
28 T. Matsubara and K. Hirao, *Organometallics*, 2001, **20**, 5759–5768.
29 P. Voyame, K. E. Toghill, M. A. Méndez and H. H. Girault, *Inorg. Chem.*, 2013, **52**, 10949–10957.
30 M. Irikura, Y. Tamaki and O. Ishitani, *Chem. Sci.*, 2021, **12**, 13888–13896.
31 Y. Tamaki, K. Koike, T. Morimoto, Y. Yamazaki and O. Ishitani, *Inorg. Chem.*, 2013, **52**, 11902–11909.
32 C. E. Castillo, J. Armstrong, E. Laurila, L. Oresmaa, M. Haukka, J. Chauvin, S. Chardon-Noblat and A. Deronzier, *ChemCatChem*, 2016, **8**, 2667–2677.
33 N. W. Kinzel, C. Werlé and W. Leitner, *Angew. Chem., Int. Ed.*, 2021, **60**, 11628–11686.
34 V. Vetere, C. Adamo and P. Maldivi, *Chem. Phys. Lett.*, 2000, **325**, 99–105.
35 C. Adamo and V. Barone, *Theor. Chem. Acc.*, 2000, **105**, 169–172.
36 C. Adamo and V. Barone, *J. Chem. Phys.*, 1999, **110**, 6158–6170.
37 M. Ernzerhof and G. E. Scuseria, *J. Chem. Phys.*, 1999, **110**, 5029–5036.
38 C. Adamo, G. E. Scuseria and V. Barone, *J. Chem. Phys.*, 1999, **111**, 2889–2899.
39 J. P. Perdew, K. Burke and M. Ernzerhof, *Phys. Rev. Lett.*, 1996, **77**, 3865.
40 M. J. Frisch, G. W. Trucks, H. B. Schlegel, G. E. Scuseria, M. A. Robb, J. R. Cheeseman, G. Scalmani, V. Barone, G. A. Petersson, H. Nakatsuji, X. Li, M. Caricato,

A. V. Marenich, J. Bloino, B. G. Janesko, R. Gomperts, B. Mennucci, H. P. Hratchian, J. V. Ortiz, A. F. Izmaylov, J. L. Sonnenberg, D. Williams-Young, F. Ding, F. Lipparini, F. Egidi, J. Goings, B. Peng, A. Petrone, T. Henderson, D. Ranasinghe, V. G. Zakrzewski, J. Gao, N. Rega, G. Zheng, W. Liang, M. Hada, M. Ehara, K. Toyota, R. Fukuda, J. Hasegawa, M. Ishida, T. Nakajima, Y. Honda, O. Kitao, H. Nakai, T. Vreven, K. Throssell, J. A. Montgomery, Jr., J. E. Peralta, F. Ogliaro, M. J. Bearpark, J. J. Heyd, E. N. Brothers, K. N. Kudin, V. N. Staroverov, T. A. Keith, R. Kobayashi, J. Normand, K. Raghavachari, A. P. Rendell, J. C. Burant, S. S. Iyengar, J. Tomasi, M. Cossi, J. M. Millam, M. Klene, C. Adamo, R. Cammi, J. W. Ochterski, R. L. Martin, K. Morokuma, O. Farkas, J. B. Foresman, and D. J. Fox, *Gaussian 16, Revision C.01*, Gaussian, Inc., Wallingford CT, 2016.

41 J. Tomasi, B. Mennucci and R. Cammi, *Chem. Rev.*, 2005, **105**, 2999–3093.

42 A. E. Reed, L. A. Curtiss and F. Weinhold, *Chem. Rev.*, 1988, **88**, 899–926.

43 F. Weinhold, Natural Bond Orbital Methods, in *Encyclopedia of Computational Chemistry*, ed. P. V. R. Schleyer, N. L. Allinger, T. Clark, J. Gasteiger, P. A. Kollman, H. F. Schaefer III and P. R. Schreiner, John Wiley and Sons, Chichester, UK, 1998, vol. 3, pp. 1792–1811.

44 S. J. A. van Gisbergen, F. Kootstra, P. R. T. Schipper, O. V. Gritsenko, J. G. Snijders and E. J. Baerends, *Phys. Rev. A: At., Mol., Opt. Phys.*, 1998, **57**, 2556–2571.

45 C. Jamorski, M. E. Casida and D. R. Salahub, *J. Chem. Phys.*, 1996, **104**, 5134–5147.

46 R. Bauernschmitt and R. Ahlrichs, *Chem. Phys. Lett.*, 1996, **256**, 454–464.

47 C. Adamo and D. Jacquemin, *Chem. Soc. Rev.*, 2013, **42**, 845–856.

48 T. B. Demissie, K. Ruud and J. H. Hansen, *Organometallics*, 2015, **34**, 4218–4228.

49 A. A. Isse and A. Gennaro, Absolute Potential of the Standard Hydrogen Electrode and the Problem of Interconversion of Potentials in Different Solvents, *J. Phys. Chem. B*, 2010, **114**, 7894–7899.

50 T. Nakajima, Y. Tamaki, K. Ueno, E. Kato, T. Nishikawa, K. Ohkubo, Y. Yamazaki, T. Morimoto and O. Ishitani, *J. Am. Chem. Soc.*, 2016, **138**, 13818–13821.

51 Y. Kuramochi, J. Itabashi, K. Fukaya, A. Enomoto, M. Yoshida and H. Ishida, *Chem. Sci.*, 2015, **6**, 3063–3074.